

A Combined Experimental and Numerical Study of the Bond between Lightweight Concrete and CFRP Bars

James V. Cox⁽¹⁾, Kristine Bergeron⁽¹⁾, and L. Javier Malvar⁽²⁾, Members ASCE

(1) Johns Hopkins University, Baltimore, MD 21218

(2) Naval Facilities Engineering Service Center, Port Hueneme, CA
james.cox@jhu.edu, bergkris@aol.com, and malvarlj@nfesc.navy.mil

Introduction

Composite materials (in particular fiber reinforced polymers – FRPs) are being applied more frequently to upgrade the civil infrastructure, but for some applications additional experimental data and studies to examine the behavior and mechanics of the structural systems are still needed. The U.S. Navy is currently applying FRPs to upgrade its waterfront reinforced concrete structures, and is considering their application as reinforcing or prestressing bars in lightweight concrete, floating structures. There is, however, little knowledge on the mechanical interaction (“bond”) between these bars and lightweight concrete. This study focuses on the bond behavior of four carbon fiber reinforced polymer (CFRP) bars within lightweight concrete. One goal of the study was to determine relevant design data such as development and transfer lengths. All of the bars considered have different surface structures (Figure 1), three of which were expected to produce significant mechanical interlocking with the adjacent concrete. In lieu of a large scale testing program, a combined experimental and numerical modeling study has been undertaken. This approach has the potential of reducing the costs of obtaining design data. This paper presents selected results of the testing program and modeling study.

The study consisted of three phases, each of which will be discussed in more detail in the following sections. In the first phase, we conducted a series of pull-out tests using an apparatus that allows different levels of confinement stress to be applied to the outer surface of a specimen (Malvar 1995). The data provide a quantitative measure of how the tangent and radial response of the specimens vary with confinement stress, which can be characterized using a bond model that adequately couples the tangent and radial responses. In the second phase of the study, we modeled the test specimens (of phase 1) for two of the bars. Models at two scales were considered, but in this paper we only report on the results for the larger scale of modeling that is amenable to the analysis of structural components. The bond model is a previously developed elastoplasticity model for characterizing the behavior associated

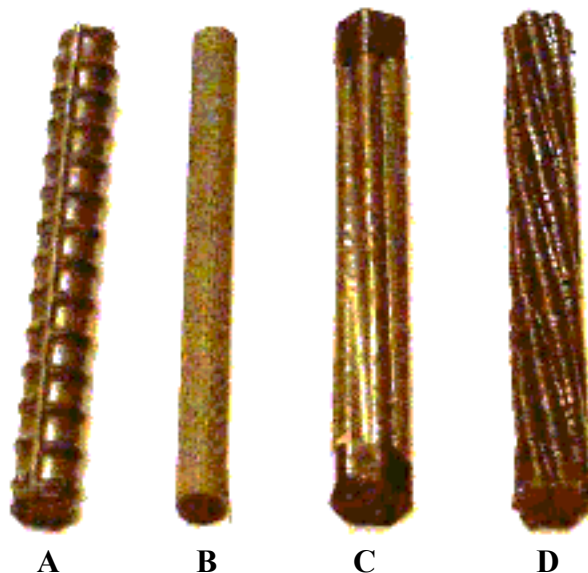


Figure 1. CFRP bar types

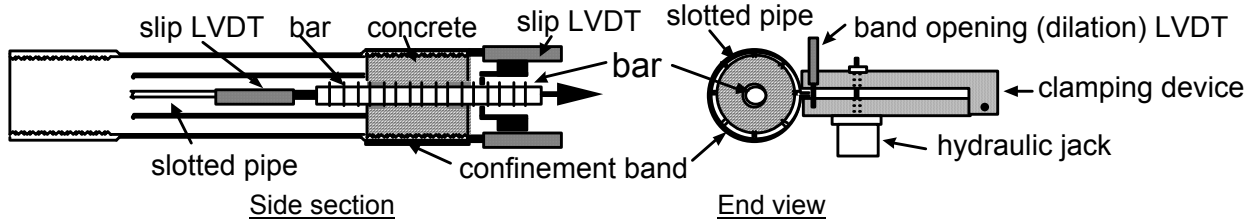


Figure 2. Schematic of Malvar test specimen.

with mechanical interlocking (Cox and Herrmann 1998). The calibrated model was recently able to reproduce the bond slip behavior of several different pull-out specimens, incorporating both GFRP (Guo and Cox 2000) and CFRP (Cox and Guo 1999) bars. The model also gave good predictions of the transfer length for a specimen using the CFRP bar (Cox and Guo 1999). The model was modified to represent the bond behavior of one of the CFRP bars examined in this study. In the third phase of the study, we conducted a limited number of pull-out tests using two different types of specimens. For these specimens, splitting failures were likely for the two bars that had exhibited the most significant mechanical interlocking.

Confinement Stress Tests

A total of fifty-three bond tests were conducted for four different bar designs using the “confinement stress specimen.” Figure 2 shows a schematic of the test arrangement. The current bond tests differ from previous tests using this apparatus in three ways: (1) multiple tests were conducted at each level of confinement stress, (2) the specimens were pre-split using a Brazilian test type setup (ASTM C496), and (3) the materials differed – lightweight concrete and CFRP bars. Multiple tests at each level of confinement stress give a better indication of the experimental scatter, and the use of a lateral load (like a split cylinder test) to pre-split the specimens was adopted to reduce the damage to the bar prior to testing. In previous tests the pre-splitting was obtained by an initial loading phase at low confinement stress, but with that approach the initial damage to the bar’s surface structure was unknown.

The specimen is a small concrete cylinder with a diameter of 3 in. (~76 mm), a length of 4 in. (~102 mm), and a bonded length of 3.0 in. (~76 mm). The specimen is cast within a slotted pipe that is later enclosed in a circumferential band. The band is used to apply compression to the outer surface of the specimen and to measure the change in circumference. The bar is loaded under displacement control in a testing frame, and a hydraulic clamp (with an adjustable relief valve) is used to apply constant confining pressure through the circumferential band. LVDTs are used to measure the longitudinal displacement at both ends of the specimen and to measure the change in circumference. For each bar type, tests were conducted with specimens subjected to four different levels of confinement stress. The intensity of the confinement stress was defined as the average radial compressive traction at the bar that would occur if the concrete did not carry hoop stress (500, 1500, 2500, and 3500 psi; *i.e.*, 3.45, 10.3, 17.2, and 24.1 MPa). The concrete was pre-split prior to performing the bond tests, so that the average normal stress at the bar would be known over a larger range of slip.

Table 1 presents data for each of the tested bars. σ_{ult} is the average ultimate strength obtained from three tensile tests. E_{long} is Young’s modulus for the longitudinal direction based upon the nominal area. L_{long} is the length (center to center spacing) of the surface structure pattern. The lightweight concrete used for the tests incorporated expanded shale for the coarse and fine aggregate. The average 28 day compressive strengths for

Table 1. Bar data.

Type	A	B	C	D
Surface	ribs – like a steel bar	textured	rope – twisted cable	rope – twisted cable
Diam.	10.2 mm (0.4 in)	8.2 mm (0.32 in)	10.6 mm (0.41 in)	9.8 mm (0.38 in)
L_{long}	7.6 mm (0.3 in)	3 mm (0.12 in)	150 mm + (6 in +)	30 mm (1.2 in)
σ_{ult}	1562 MPa (228 ksi)	1456 MPa (211 ksi)	1931 MPa (280 ksi)	1871 MPa (271 ksi)
E_{long}	113 GPa (16,400 ksi)	139 GPa (20,200 ksi)	157 GPa (22,800 ksi)	137 GPa (19,900 ksi)

the different batches ranged from 34.5-51 MPa (5000-7400 psi), and average splitting tensile strengths ranged from 3.2-4.5 MPa (460-660 psi).

Figure 3 presents typical bond responses for all four bars at two different values of $-\sigma$. The textured surface of the type B bar has a “relatively insignificant structure,” yet the effects of mechanical interlocking are evident in the response – τ “cycling” on a slip interval of approximately L_{long} . However, the dilation produced by the interlocking was not large enough to open the longitudinal cracks, and thus there was no apparent correlation between σ and τ_{max} . An additional limitation of the current apparatus is that it does not offer restraint against twisting. The torsional stiffness of the CFRP bars is relatively low, so the twisted cable type bars tended to “unscrew” from their helical cavities in the concrete. We expect that this behavior produced smaller radial dilations and bond stresses than would occur if the twisting motion was restrained.

In terms of using the test data to calibrate a bond model, the tests were most effective for the type A bar. Among the important trends in the experimental data are the increase in τ and the decrease in δ_n with an increase in confinement stress. While the same general trends have previously been observed for steel bars, the bond failure mechanisms for FRP bars can be significantly different since the surface structure of the bar itself can fail. Figure 4 shows photographs of the undamaged surface structure and the damaged surface

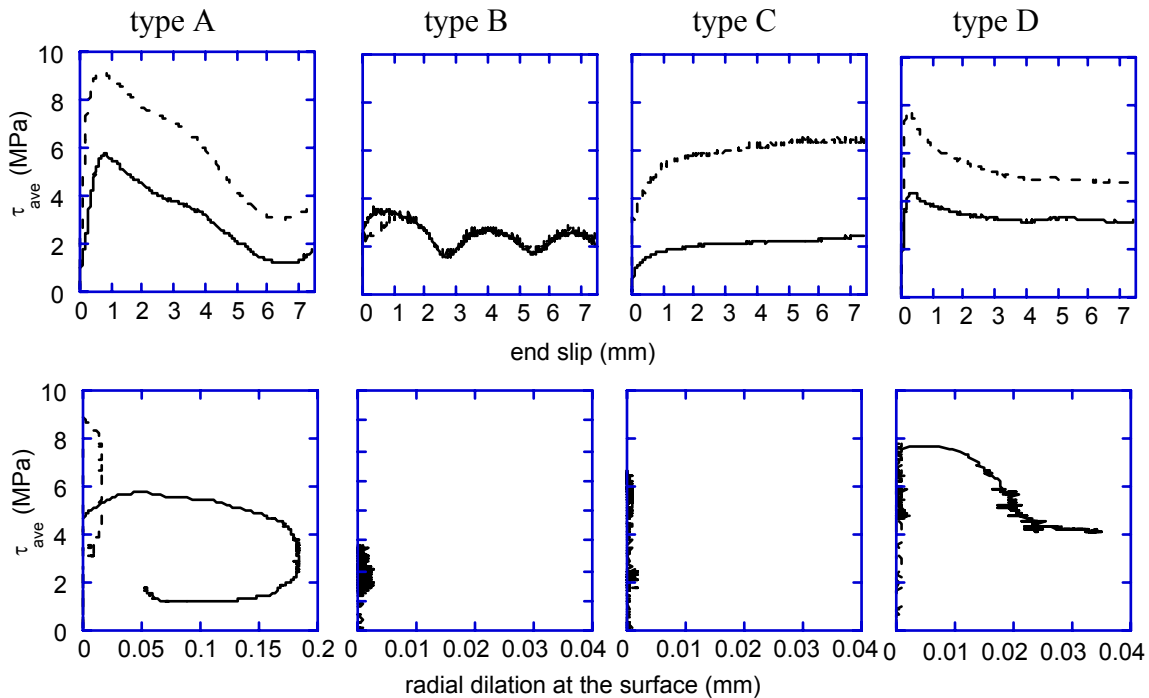


Figure 3. Bond stress (τ) vs. end slip and radial dilation at the surface. solid line $\sim \sigma=1500$ psi (10.3 MPa), dashed line $\sim \sigma=3500$ psi (24.1 MPa)

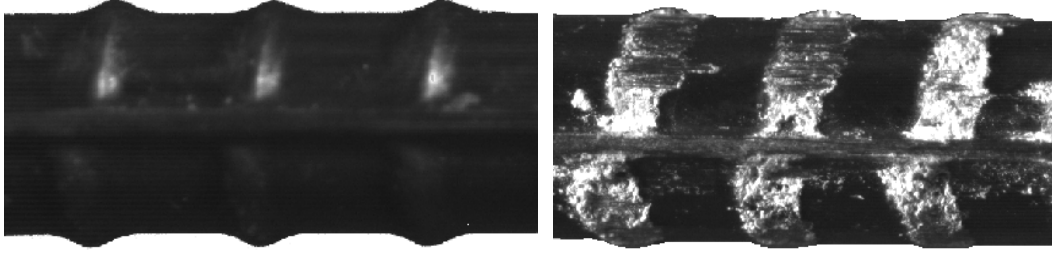


Figure 4. Original and damaged surface structures of the type A bar.

structure for a type A bar tested with $\sigma=2500$ psi (17.2 MPa). It appears that the reduction of the wedging action of the ribs at higher confinement stresses is due more to increased surface structure damage than concrete crushing.

Bond Modeling

Of the four bar types two were selected for additional numerical studies – types A and D. The numerical component of the study includes modeling of the bond behavior at two scales: one to examine the progressive failure that results from the mechanical interlocking, and the second to characterize the bond behavior at a scale amenable to the analysis of structural components. This paper addresses the latter scale of modeling (for the type A bar) which adopts a previously developed elastoplastic bond model (Cox and Herrmann 1998).

The generalized stresses (\mathbf{Q}) for the model are the tangent (τ) and normal (σ) components of the interface traction. The generalized strains (\mathbf{q}) are defined as the tangent (δ_t) and normal (δ_n) displacements of the concrete surface measured relative to the bar surface and nondimensionalized by the bar diameter (D_b); *i.e.*, $\mathbf{q}^T = (\delta_t/D_b, \delta_n/D_b)$. For the problems, examined in this study the applied forces are assumed to be longitudinal (*i.e.*, doweling forces are not considered).

For monotonic loading, the yield surface and flow rule evolutions are characterized by a single internal variable, the *interface degradation* – $d = \min(\delta_t^p/s_r, 1)$ where δ_t^p is the plastic slip and s_r is a characteristic length of the surface structure (*e.g.*, rib spacing). The yield criterion is of the form: $f(\tau, \sigma, d) = 0$ where

$$f(\tau, \sigma, d) = \left| \frac{\tau}{f_t} \right| - C(d) \left\{ W_e(d) \left[1 - e^{-\alpha_e(-\sigma/f_t + \hat{\sigma}(d))} \right] + M(1 - W_e(d)) \left| \frac{-\sigma}{f_t} + \hat{\sigma}(d) \right|^{\alpha_p} \operatorname{sgn} \left(\frac{-\sigma}{f_t} + \hat{\sigma}(d) \right) \right\} \quad (1)$$

f_t is the tensile strength of concrete; C is the isotropic hardening/softening function; $\hat{\sigma}$ is the kinematic softening function; W_e is the “morphing function” between the two shapes of the yield surface; M , α_p and α_e are model parameters.

The flow rule produces dilation of the interface, representing the inelastic, relative, radial displacement that results from the mechanical interlocking of the bar’s surface structure with the adjacent concrete. An important experimental behavior reproduced by the flow rule is the decrease in radial dilation with an increase in confinement stress. This element of the model provides the potential for predicting both pull-out and splitting failures. Additional details on the form of the model and upon how the phase 1 data can be used for calibration are given by Cox and Herrmann (1998).

Figure 5 shows comparisons of experimental results for the type A bar and the behavior predicted by the calibrated model. Each specimen is modeled using axisymmetric finite elements, and the bond model is used to describe the behavior of the interface between the bar and concrete. The coefficients of variation in the experimental data for bond strength range from 0.14 to 0.57 and for maximum dilation (for the types A and D bars) they range from 0.06 to 0.96. The calibrated model represents the overall trends in the experimental data, but certainly some details of the behavior are not captured.

Splitting Predictions

With the bond model calibrated, it was then used to predict the behavior of two types of specimens (for the type A bar): an unsplit phase 1 specimen, and a long embedment length specimen (152 mm diameter, 610 mm length, and 533 mm bonded length). For these specimens the longitudinal cracking in the concrete was modeled using a fictitious crack model (Hillerborg *et al.* 1976), adopting the exponential traction-crack opening relationship of Reinhardt *et al.* (1986). The cracks were incorporated into the axisymmetric models using the approach of Rots (1988).

Experimental measurements of the fracture properties of the concrete were limited to the splitting tests. Based on the experimental study of Cornelissen *et al.* (1986), the splitting strength for lightweight concrete is significantly different than the direct tensile strength – in their case about 150%. The fracture energy associated with the cracks was assumed to be 75 J/m², the critical crack opening was assumed to be 0.14 mm, $f_t = 3$ MPa, and the number of cracks is a model parameter.

Figure 6 compares the model and experimental results for the confinement specimen with $\sigma = -500$ psi. These specimens failed with four longitudinal cracks, and the model prediction based on four cracks falls just below the experimental scatter.

Table 2 compares the model and experimental bond strengths for

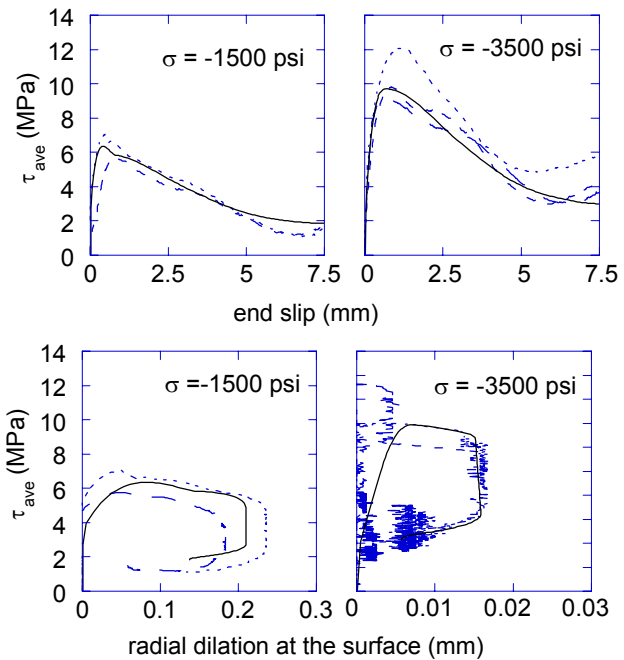


Figure 5. Model calibration results at two confinement levels (solid line ~ model).

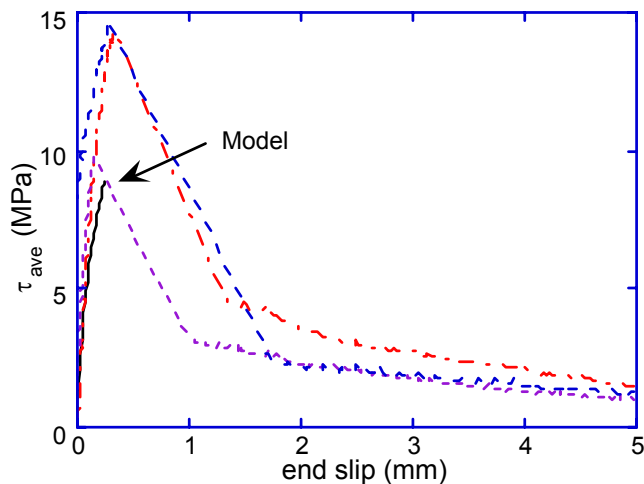


Figure 6. Splitting test with $\sigma = -500$ psi. (solid line ~ model)

Table 2. Bond Strength (τ_{\max}) for 2 ft specimens, type A bars.

Experimental		Model		
Test no. 1	Test no. 2	1 crack	2 cracks	3 cracks
3.95 MPa	6.10 MPa	2.9 MPa	4.3 MPa	5.9 MPa

the long embedment specimen. These specimens failed with three longitudinal cracks, and the model result for three cracks falls within the experimental scatter.

Conclusions

The apparatus for measuring the confinement stress dependent bond response was effective for the type A bar but may need to be restrained from twisting for bars with a helical structure. The effects of mechanical interlocking were experimentally observable even for a type B bar which has a finely textured surface, but the specimen size was too large to measure the effects of the stress state upon the bond response for this bar. The calibrated bond model gave reasonable predictions of the splitting strength for two different types of pull-out specimens, when the number of longitudinal cracks for the failed specimen was used in the model.

Acknowledgments

Support for this study by the National Science Foundation (grant no. CMS-9872609), the Naval Facilities Engineering Service Center (contract no. N0024498P0366), and the Office of Naval Research are gratefully acknowledged. CFRP bars were provided by: Marshall Industries Composites, Inc.; Prof. Charles W. Dolan, University of Wyoming; and Prof. Srinivasa L. Iyer, South Dakota School of Mines and Technology.

References

- Cornelissen, H.A.W., Hordijk, D.A., and Reinhardt, H.W. (1986). "Experiments and theory for the application of fracture mechanics to normal and lightweight concrete," *Fracture Toughness and Fracture Energy of Concrete*, Elsevier Science Publishers, 565-575.
- Cox, J.V. and Herrmann, L.R. (1998). "Development of a plasticity bond model for reinforced concrete," *Mech. of Cohesive-Frictional Mat.*, 3:155-180.
- Cox, J. and Guo, J. (1999). "Modeling the stress state dependency of the bond behavior of FRP tendons," *Fourth International Symposium on FRP for RC Structures*, SP-188, American Concrete Institute (ACI), C.W. Dolan, S.H. Rizkalla, and A. Nanni, eds., SP 188-68, 791-805.
- Guo, J. and Cox, J.V. (2000). "An interface model for the mechanical interaction between FRP bars and concrete," *Journal of Reinforced Plastics and Comp.*, 19(1):15-33.
- Hillerborg, A., M. Modéer, and Petersson, P.A. (1976). "Analysis of crack formation and crack growth in concrete by means of fracture mechanics and finite elements," *Cement and Concrete Research*, 6:773-782.
- Malvar, L.J. (1995). "Tensile and bond properties of GFRP reinforcing bars." *ACI Materials Journal*, 92(3):276-285.
- Reinhardt, H.W., Cornelissen, H.A.W., and Hordijk, D.A. (1986). "Tensile tests and failure analysis of concrete," *Journal of the Structures Division, ASCE*, 112(11):2462-2477.
- Rots, J.G. (1988). *Computational Modeling of Concrete Fracture*, Ph.D. dissertation, Delft University of Technology, Delft.